



ISSN NO. 2320-5407

Journal homepage: <http://www.journalijar.com>

INTERNATIONAL JOURNAL
OF ADVANCED RESEARCH

RESEARCH ARTICLE

Dielectric Spectroscopy Studies in Zn_2FeNO_3 , Zn_2AlNO_3 and $Zn_2Fe_{0.5}Al_{0.5}NO_3$

A. ELMELOUKY¹, A. MORTADI¹, R. ELMOZNINE¹, R. LAHKALE², EL. SABBAR², E.G. CHAHID¹,

1. Laboratoire de Physique de La Matière Condensées(LPMC). Université Chouaib Doukkali, Faculté des Sciences, El-Jadida, Morocco

2. Laboratoire de Physicochimie des matériaux(LPCM). Université Chouaib Doukkali, Faculté des sciences, El-Jadida, Morocco

Manuscript Info**Manuscript History:**

Received: 15 September 2015

Final Accepted: 22 October 2015

Published Online: November 2015

Key words:

LHD, Dielectric, Impedance, Electric, Modulus, Conductivity.

***Corresponding Author**

ELMELOUKY

Abstract

Dielectric response, impedance, modulus, dc and ac conductivity of hydroxide double lamellar (LDH), $[Zn_2AlNO_3]$, $[Zn_2FeNO_3]$ and $[Zn_2Fe_{0.5}Al_{0.5}NO_3]$ at room temperature and at frequency range (1Hz-1MHz). LDH prepared by the co-precipitation technique, the results of X-ray diffraction confirmed the partial and overall substitution of Al by Fe.

The space group does not change neither the structure also. The dielectric analysis reveals the presence of electrode polarization, free charge motion at low frequencies which are related to space charge polarization and Conductivity relaxation respectively. Complex impedance plots (Cole-Cole plots) showed a non-Debye type relaxation. These are resolved into two semicircles, indicating the bulk, grain boundary. Modulus studies confirm the conductivity effect by hopping and localized motion of ions.

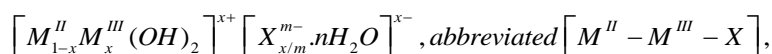
The frequency dependence of the electric conductivity was found to follow a double power law behavior, in accordance with the relation $\sigma'(\omega) = \sigma_{dc} + A_1\omega^{S_1} + A_2\omega^{S_2}$, where S_1 and S_2 are smaller than 1.

Copy Right, IJAR, 2015.. All rights reserved

INTRODUCTION

In layered double hydroxides (LDH), have received extensive research in recent years. Interests in such materials rest in their remarkably broad spectrum of chemical, structural, physical and mechanical properties leading to numerous practical applications. The new developments of the applications of organo-exchanged LDH include the immobilization of photo and electro-active species, the complexation with organic polymers for the enhancement of mechanical properties and the selective adsorption of toxic compounds from water (M. Lakraimi et al 2003) as well as their use as pharmaceutical products, catalysts and gene delivery vectors (V. Rives 2001).

LDH, also called anionic (anion exchanging) clays or hydrotalcite-like compounds (R. Allmann 1970), consist of brucite-like materials, where a fraction of the divalent cations have been replaced isomorphously by trivalent cations giving positively charged layers and interlayer charge compensating anionic species or counter ions between the layers. Some hydrogen bonded water molecules may occupy the remaining free space of the interlayer domain. These materials are described according to the ideal formula:



Where M^{II} and M^{III} are divalent and trivalent metal ions, respectively, X_m the interlayer anion and x is defined as the $M^{II} / (M^{II} + M^{III})$ ratio. For LDH prepared with ternary cations, its general formula is the stacked sheets are held together by weak interactions via hydrogen bonding and the anions, which are accompanied by water molecules in the interlayer domain, are exchangeable.

This work focuses on the study of electrical properties of $[Zn_2FeNO_3]$, $[Zn_2AlNO_3]$ and $[Zn_2Fe_{0.5}Al_{0.5}NO_3]$ (LDH) by impedance spectroscopy and dielectric. By analyzing experimental data by well-defined representations to determine the different dielectric relaxations of the LDH. In addition, we present the results on the AC conductivity and DC. The relaxation gives us information on the storage of energy.

Studies on the conductivity of all samples are important in order to gain a better insight on the ionic conduction mechanism especially in its usage cathode materials. Dielectric and impedance spectroscopy is widely used for investigating the electrical and electrochemical properties (El melouky & al). The application of AC technique of complex impedance analysis is important and eliminates pseudo effects if any in the material. Complex impedance analysis makes it possible to separate the contribution due to grain, grain boundary and interfacial effects. Generally, these properties depend on the resistive and capacitive components in the material. So that, the result obtained from these analyses provide true representation of electrical behavior of the sample. In case of the electrical properties of the oxides, grain boundaries play an important role. The measurement of conductivity and impedance shows dispersion behavior which offers an opportunity to gain some information of ionic migration process. Considering the significance, the electrical conductivity studies on various of the quantity of metal trivalent (Al or Fe) in $[Zn_2FeNO_3]$, $[Zn_2AlNO_3]$ and $[Zn_2Fe_{0.5}Al_{0.5}NO_3]$ (LDH).

1. Experimental of Zn_2FeNO_3 , Zn_2AlNO_3 and $Zn_2Fe_{0.5}Al_{0.5}NO_3$

The $[Zn_2FeNO_3]$ and $[Zn_2Fe_{0.5}Al_{0.5}NO_3]$ matrices were synthesized separately by the constant pH coprecipitation method. Salts of $ZnCl_2$ ($AlCl_3 \cdot 6H_2O$), $(Fe(NO_3)_3 \cdot 9H_2O)$ such that the molar ratio of $Zn^{2+} / Fe^{3+} = 2$ for $[Zn_2FeNO_3]$ and $[Zn_2AlNO_3]$ matrix with $Fe^{3+} / Al^{3+} = 1$ for matrix $[Zn_2Fe_{0.5}Al_{0.5}NO_3]$. Once prepared and dissolved salts in decarbonated water, adding them to a solution of NaOH freshly prepared in decarbonated water should be done under nitrogen dropwise while maintaining the pH at 8. After pouring all of the solution of salts, the obtained colloidal mixture is stirred for 24 h, washed thoroughly several times with decarbonated water, then dried $60^\circ C$ for 48 h and ground to end for analysis.

The X-ray diffraction patterns were carried out on **D2-PHASER** of **BRUKER-AXS diffractometer** which used $K\alpha_1$ (1.54056 \AA) and $K\alpha_2$ (1.54439 \AA). Generator used at 30 kV and 10 mA. Computation time 15 and 70° (2θ) by step of 0.0101° (0.2 s by step). Program duration is 18mn 06 s.

The measurements were performed using a transform spectrometer FT-IR-Spectrometer SHIMADZU 8400S. The samples are conditioned in the form of pellets 13 mm in diameter, consisting of 1.8 mg of the product diluted in 200 mg of KBr (support). The results are shown in absorbance wave numbers between 4000 and 400 cm^{-1} . The resolution is 2 cm^{-1} and the number of scans 20

Thermogravimetric measurements were made using microbalance TG-DTA SETARAM 92.

The impedance measurements were carried out with a Solartron HP (Hewlett Packard) Impedance analyzer between 1 Hz and 1 MHz a source of 1V was applied to the electroded pellet samples.

The diameter and the thickness of the sample were 13 mm and 1 mm, respectively. Curve fitting of dielectric spectra with complex empirical functions was carried out using commercial « ZviewTM » software (version 2.2) and non-linear fitting curve by origin Lab.

I.2.Characterization by XRD

The diffraction X patterns for all compounds [Zn_2FeNO_3], [Zn_2AlNO_3] and [$\text{Zn}_2\text{Al}_{0.5}\text{Fe}_{0.5}\text{NO}_3$] are characteristic of a hexagonal lattice with rhombohedral symmetry, and all the lines are indexables in the space group R-3m (Roussel, H., et al. 2000).

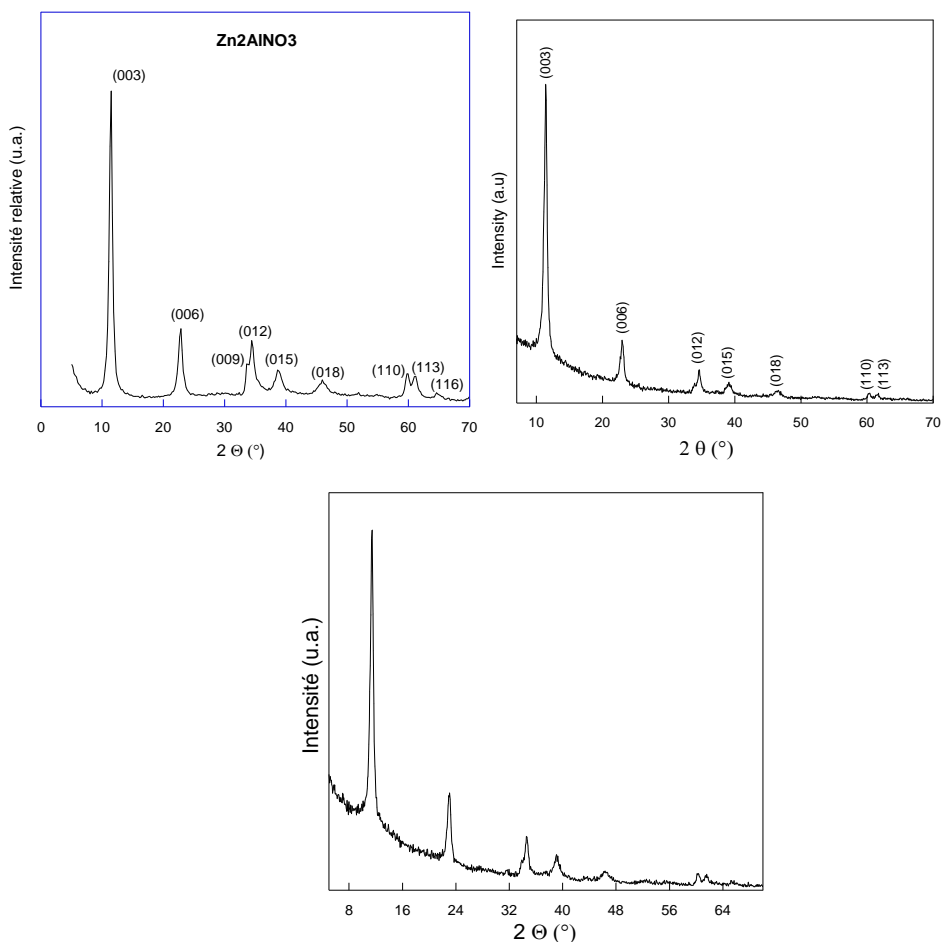


Figure 1. XRD Spectrum of Zn_2AlNO_3 , Zn_2FeNO_3 and $\text{Zn}_2\text{Al}_{0.5}\text{Fe}_{0.5}\text{NO}_3$

The angular position of the first diffraction peak (003) is connected to the spacing of the sheet, and allows the calculation of the parameter c ($c = 3d_{003} = 6d_{006}$) or on the average of the first two harmonics, $c/3 = 1/2 (2d_{006} + d_{003})$. The stripe (110) located in the vicinity of 60° in 2Θ is connected to the parameter by the relation $a = 2d_{110}$ (Rousselot, I., and al, 2002). It allows us to determine the value of the parameter a , that is to say, the metal-metal distance in the slip. In Table 1 we give the lattice parameters of the three test compounds based solely on data of the X-ray diffraction.

Table 1. Results lattice parameters found by XRD

Matrices (HDL)	c (Å°)	a (Å°)	d _{inter} (Å°)
Zn ₂ AlNO ₃	23.88	3.10	7.96
Zn ₂ FeNO ₃	23.29	3.09	7.76
Zn ₂ Fe _{0.5} Al _{0.5} NO ₃	23.15	3.06	7.71

The values of these parameters vary from one phase to another, the parameter is modified by the nature and the ionic radius of the cation own sheet but also the substitution rate of trivalent metal (A. Mantilla and al 2009) variation of the parameter c is related to the nature, direction and charge of intercalated anions, and the type of links created with the leaves and the rate of hydration. Note that the parameters **a** and **c** decreases when the dope Iron 50% Al. Indeed, the ionic radius of Al³⁺ is less than that of Fe³⁺ ($r(\text{Al}^{3+}) = 0.50 \text{ \AA}$ ($r(\text{Fe}^{3+}) = 0.64 \text{ \AA}$).

I.3. Infrared Spectroscopy

The corresponding IR spectrum (Fig. 2) presents profiles that resemble those exhibited by all samples phases.

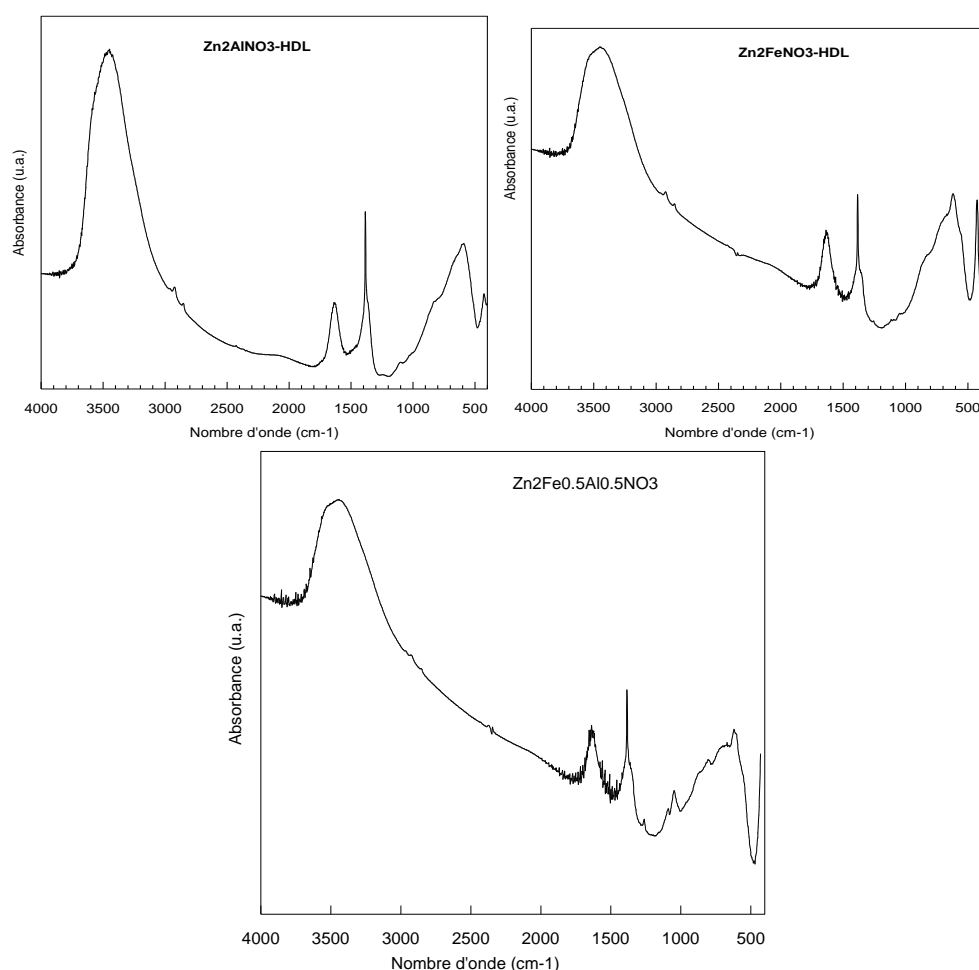


Figure.2. Infrared Spectroscopy of Zn₂AlNO₃, Zn₂FeNO₃ and Zn₂Al_{0.5}Fe_{0.5}NO₃

- The broad and intense band corresponding to the stretching vibration ν (OH).
- The low intensity band corresponding to the vibration of deformation δ (H₂O).
- ν (NO₃⁻) is the one nitrate stretching vibration band characterized by very intense.

- ν (M-O) and δ (O-M-O) respectively correspond to the vibration and deformation of valence of clay slip (M is Zn, Al and Fe).

Tableau.2. Absorbance bands of frequencies and powers in Zn_2FeNO_3 , $Zn_2Fe_{0.5}Al_{0.5}NO_3$ and Zn_2AlNO_3

Samples LDH	ν (OH) (cm ⁻¹)	δ (H ₂ O) (cm ⁻¹)	ν (NO ₃ ⁻) (cm ⁻¹)	ν (M-O) (cm ⁻¹)	δ (O-M-O) (cm ⁻¹)
Zn_2AlNO_3	3448.8	1637.6	1384.9	590.24	428.21
Zn_2FeNO_3	3454.91	1636.32	1385.61	619.68	426.89
$Zn_2Fe_{0.5}Al_{0.5}NO_3$	3431.5	1633.1	1379.1	621.10	428

Infrared spectra shown in Fig.2 in the range of 400-4000 cm⁻¹ of the synthesized compounds are typical of what is generally observed for HDL phases. The various bands of molecular vibrations and network are identifiable on each Spectrum.

The infrared spectra of all matrices have a broad and intense band centered around 3448. 8 cm⁻¹ (Zn_2AlNO_3) and 3454.91 cm⁻¹ (Zn_2FeNO_3) and 3431.5 cm⁻¹ ($Zn_2Fe_{0.5}Al_{0.5}NO_3$), corresponding respectively to the vibration valence and interaction forces ν hydroxyl (OH). The observed shift in the position of this band is probably due to the difference in composition and in particular to the differences noted in the report (M^{II} / M^{III}) between these two phases. The town band for all LDH is the absorption at 1637.6; 1636.32 and 1633.1 cm⁻¹ assigned to the vibration of deformation respectively (Zn_2AlNO_3), (Zn_2FeNO_3) and ($Zn_2Fe_{0.5}Al_{0.5}NO_3$).

The values of these parameters vary from one phase to another, the parameter is modified by the nature and the ionic radius of the cation own sheet but also the substitution rate of trivalent metal (M. Lakraimi and al 2006).

The variation of the parameter c is related to the nature, direction and charge of intercalated anions, and the type of links created with the leaves and the rate of hydration. Note that the parameters a and c decreases when the dope Iron 50% Al. Indeed, the ionic radius of Al³⁺ is less than that of Fe³⁺ (r (Al³⁺) = 0.50 Å (r (Fe³⁺) = 0.64 Å).

In the low frequency region, that is to say for $\nu < 800$ cm⁻¹, there are the vibration characteristics of the network. Infrared spectra reflect differences in the nature of the metal cations present in the hydroxyl layers of the two matrices. The exact positions of these vibrations on the frequency scale, as well as their assignment to specific normal modes are tabulated table.2. We can distinguish two types of vibration ν (M-O) between the metal and the oxygen atoms forming the octahedron hydroxyl, as well as vibration of deformation of oxygen-metal-oxygen bonds δ (O-M-O) octahedral is joined. On the other hand, one can also note here that the relatively broad shape of these bands can be attributed to a domain interlamellar disorganized.

I.4. ICP analysis

The metallic ratio what were performed using ICP measurements. A plasma or gas consisting of ions, electrons and neutral particles, is formed from Argon gas, which is then utilized to atomize and ionize the elements in the sample matrix. These resulting ions are then passed through a series of apertures into a high vacuum mass analyzer where the isotopes of the elements are identified by their mass-to-charge ratio The intensity of a specific peak in the mass spectrum is proportional to the amount of the elemental isotope from the original sample, this technique of choice in many analytical for providing the accurate and precise measurements. Table (3) combines the different results obtained.

Table3. H₂O content in matrices Zn_2FeNO_3 , Zn_2AlNO_3 and $Zn_2Fe_{0.5}Al_{0.5}NO_3$ initial masses and masses of losses for each compound

Samples LDH	m_i (initial weight) (mg)	m_p (mass loss) (mg)	% d'H ₂ O = 100($\Delta m / m_i$)
Zn_2AlNO_3	50	7	14
Zn_2FeNO_3	50	7	14
$Zn_2Fe_{0.5}Al_{0.5}NO_3$	50	6.42	12.85

I.5. TGA of the Compounds Zn_2FeNO_3 , $Zn_2Al_{0.5}Fe_{0.5}NO_3$ and Zn_2AlNO_3

Thermogravimetric analysis enables us to determine the different thermal events during heating. In general, the thermal evolution LDH phase involves three main events for $[Zn_2FeNO_3]$, $[Zn_2AlNO_3]$ and $[Zn_2Al_{0.5}Fe_{0.5}NO_3]$.

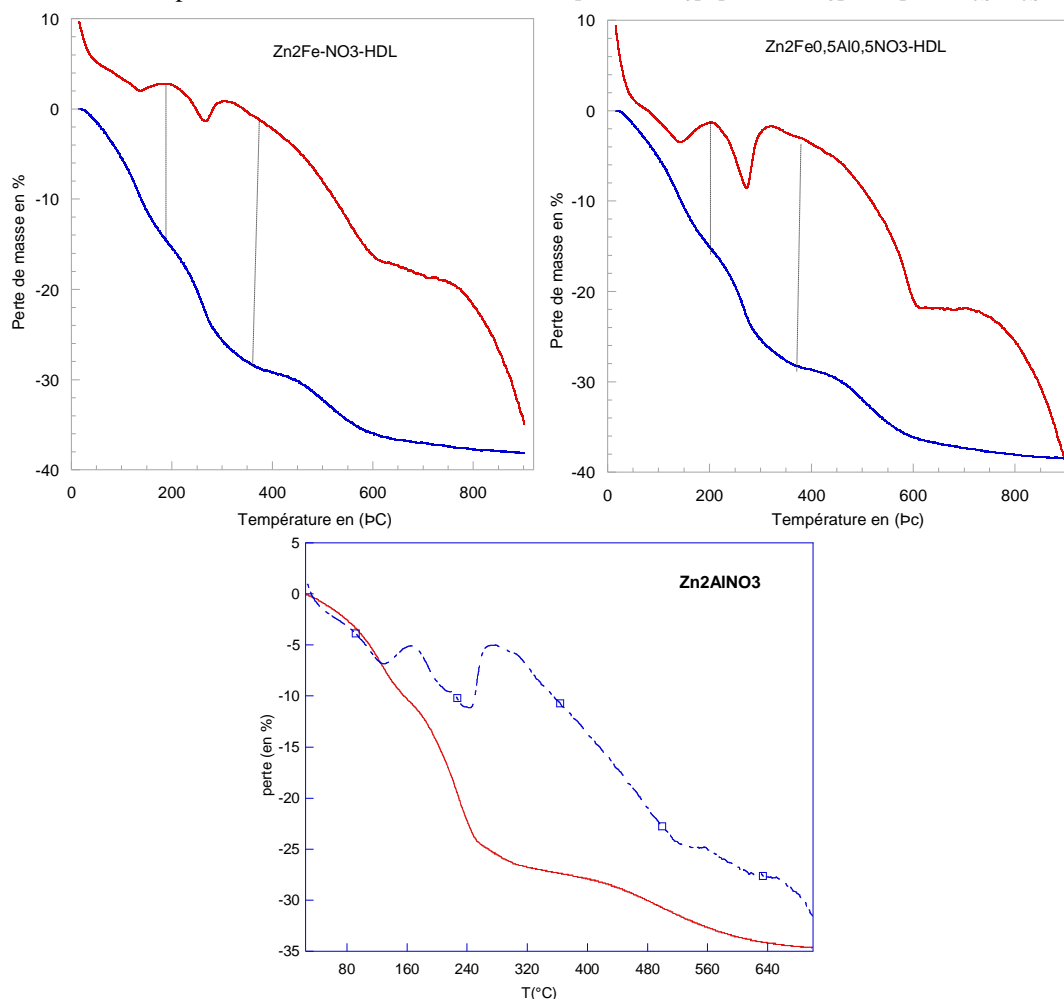


Figure 7: TGA curve for Zn_2FeNO_3 , $Zn_2Al_{0.5}Fe_{0.5}NO_3$ and Zn_2AlNO_3

The phases of thermal images $[Zn_2FeNO_3]$ and $[Zn_2Al_{0.5}Fe_{0.5}NO_3]$ shown in Figure 7 can distinguish three stages of thermal decomposition, respectively.

The first step is the loss of adsorbed water interlamellar water, it is between $15.6^\circ C$ and $185.61^\circ C$ for $[Zn_2FeNO_3]$ phase with a weight loss of 14.39%, and between $15.6^\circ C$ and $201.75^\circ C$ for $[Zn_2Al_{0.5}Fe_{0.5}NO_3]$ phase with a weight loss of 15.15%, from $185.61^\circ C$ is the dehydroxylation is predominant for $[Zn_2FeNO_3]$, it occurs at a temperature lower than that observed for phase $[Zn_2Al_{0.5}Fe_{0.5}NO_3]$, it accelerates from 215 to $360.4^\circ C$ for $[Zn_2FeNO_3]$ between 226 and $371.22^\circ C$ of $[Zn_2Al_{0.5}Fe_{0.5}NO_3]$. The mass losses identified on TGA curves (14% $[Zn_2FeNO_3]$ and 12.85% for $[Zn_2Al_{0.5}Fe_{0.5}NO_3]$).

Above $360.4^\circ C$, manifests the start of nitrates for $[Zn_2FeNO_3]$, and $371.22^\circ C$ of $[Zn_2Al_{0.5}Fe_{0.5}NO_3]$.

The above results make it possible to say that the matrix $[Zn_2FeNO_3]$ is somewhat stabilized by the effect the doping of Al. TGA for $[Zn_2AlNO_3]$ are marked by a first mass loss between room temperature and $200^\circ C$ due to the departure of water molecules intercalated and adsorbed to the surface. The following loss that ends at $310^\circ C$ is

the departure of hydroxyl ions of the cationic constituent sheet, then the decomposition of the intercalated anion which ended around 660°C.

I.6. Dielectrical Study

I.6.1. Complex impedance representation

The application of the A.C technique of the complex impedance analysis (P. Rosaiah and al 2013), eliminates the pseudo effects, if any, in the material electrical properties by separating out the real and imaginary parts of the material electrical properties. It has unique feature to investigate the electrical properties of a material, which are independent of the sample geometrical factors and there by enables a better correlation of electrical properties with sample microstructure (Jingwen Yao and al 2013).

Complex impedance diagrams have been found to be very useful to distinguish the contribution of resistivity from grain and grain boundaries of polycrystalline sample having different time constants in frequency domain (P. Rosaiah and al 2013). Impedance spectroscopy is promising nondestructive testing method for analyzing ferroelectrics and piezoelectrics. The literature survey indicates lot of work in variety of materials has been characterized for electrical properties using complex impedance and modulus formalism (Chahid and al 2013).

Shows in fig. 8 the impedance plot the imaginary part Z'' as a function of real part Z' measured and fitted by equivalent circuit fig. 9. at a substitution of Al metal by Fe metal at room temperature in the frequency range (1Hz-1MHz). This diagram shows the appearance of two semi circles in the Cole-Cole plots indicates that there are two relaxation mechanisms, which may be due to grain and grain boundary. As the sample $Zn_2Fe_{0.5}Al_{0.5}NO_3$ all the semicircles became smaller and shift towards lower Z indicating a reduction in the resistance of both the grain and grain boundary. For comparative study of Zn_2FeNO_3 and Zn_2AlNO_3 , indicating reduction in the resistance of both the grain and grain boundary where substitution Al by Fe. Hence, grain and grain boundary effects could be separated. In case of HDL, this is commonly grain boundaries are insulating and grain is semi conductive grains.

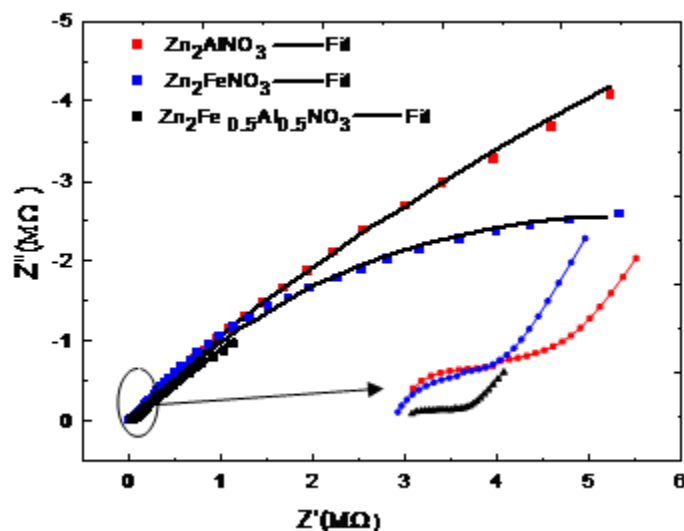


Figure 8: Cole-Cole plots of Zn_2AlNO_3 , Zn_2FeNO_3 and $Zn_2Fe_{0.5}Al_{0.5}NO_3$

The impedance data can be represented as an equivalent circuit consisting of two parallel (R // CPE) elements in series fig. 9. (A. Ali Ahmed and al 2012), (H.Kavas and al 2009). This is the one of the most common interpretation for polycrystalline materials having a contribution of grain (bulk) and grain boundary in series.

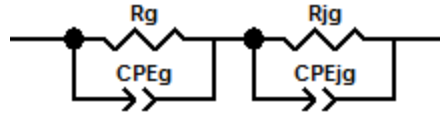


Fig. 9. Equivalent circuit

The impedance of the circuit is given by:

$$Z^*(\omega) = Z_g^*(\omega) + Z_{jg}^*(\omega)$$

$$Z^*(\omega) = \frac{R_g}{1 + (j\tau_g \cdot \omega)^{p_g}} + \frac{R_{jg}}{1 + (j\tau_{jg} \cdot \omega)^{p_{jg}}}, \quad \tau_g = (R_g T_g)^{1/p_g} \quad \text{and} \quad \tau_{jg} = (R_{jg} T_{jg})^{1/p_{jg}}$$

τ_g and τ_{jg} represents respectively the measure of the width of the distribution of the relaxation time. The value of (τ_g , τ_{jg}) estimated from the Cole-Cole plots.

In general, the impedance of a CPE is expressed via the following complex equation (Huebner and al.1995):

$$Z_{CPE} = \frac{1}{T(j\omega)^p} \quad \text{Where the exponent } p \text{ may vary from } 0 \text{ for pure resistive to } +1 \text{ for pure capacitive behavior.}$$

Where $\omega = 2\pi f$ is the angular frequency and T_i and p_i refer to CPEi parameters. These parameters were estimated for each spectrum during the substitution and are summarized in table 2 for the corresponding Cole–Cole plots in fig. 8. As it is seen, the fitting curves (solid lines in fig. 8) exhibit very good correlation with the experimental data.

Generally, the arc at high frequency end refers to bulk and at low frequency end refers to grain boundary. The resistance of bulk or grain (R_g), grain boundary (R_{jg}) could directly be obtained from intercept on the Z' axis. In Table 2 can be seen the decrement in the grain and grain boundary resistance is attributed to the conduction mechanism at the grain – grain boundary.

Table 2: Fitting parameters of the equivalent circuit for the Cole–Cole plots of complex impedance shown in fig. 8.

Samples(LDH)	Tg	Pg	Rg(ohm)	Tjg	Pjg	Rjg(ohm)
Zn ₂ AlNO ₃	8.03 E-11	0.86	46893	3.77E-8	0.78	5E7
Zn ₂ FeNO ₃	6.80 E-11	0.91	35477	3.4E-8	0.57	5.02 E6
Zn ₂ Fe _{0.5} Al _{0.5} NO ₃	5.45 E-10	0.74	25909	4.7 E-7	0.52	1.57E6

1.6.2. Complex Conductivity Measurements

The real parts of the total conductivity $\sigma(\omega)$ are calculated using the following expressions:

$$\sigma'(\omega) = \frac{L}{S} \frac{Z'}{Z'^2 + Z''^2}$$

Where L , S , Z' and Z'' are the thickness, the cross section area and the real and imaginary parts of the complex impedance.

Fig.10 shows the variation of ac conductivity with frequency for the [Zn₂AlNO₃], [Zn₂AlNO₃] and [Zn₂Fe_{0.5}Al_{0.5}NO₃] composition at room temperature. The ac conductivity patterns show a frequency independent plateau in the low frequency region and exhibits dispersion at higher frequencies and medium frequencies. This behavior obeys the universal double power law (Banarji Behera, and al, 2013), (A.S.Dzunuzvie and al, 2015)

$\sigma'(\omega) = \sigma_{dc} + A_1 \omega^{n_1} + A_2 \omega^{n_2}$, (the solid line is the fit to the expression) where σ_{dc} is the dc conductivity (frequency independent plateau in the low frequency region), A_1 and A_2 is the pre-exponential factor, n_1 and n_2 is the fractional exponent between 0 and 1.

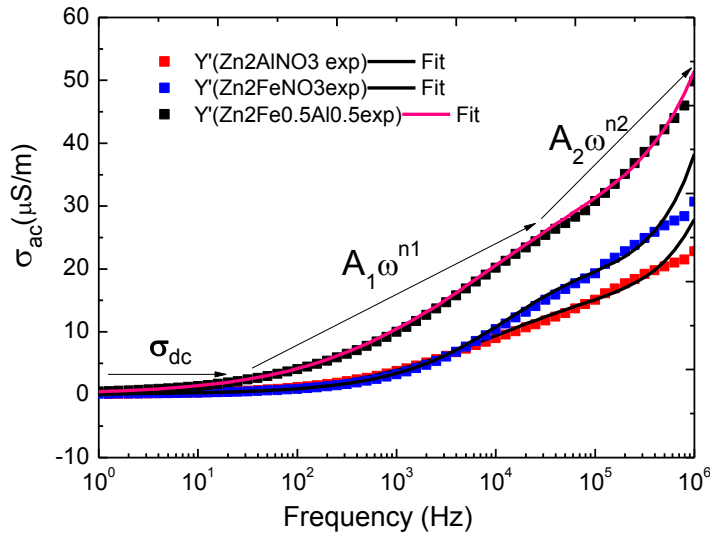


Figure 10: Variation of σ_{ac} conductivity as a function of frequency

The deviation from, dc (plateau region) value in the conductivity spectrum (in the low frequency region) is due to the electrode polarization effect. The values of A_1 , A_2 , n_1 and n_2 were obtained by fitting curve by origin Lab the $\sigma'(\omega) = \sigma_{dc} + A_1\omega^{n_1} + A_2\omega^{n_2}$ (A. Langar and al, 2014) is tabulated in Table 3.

The bulk conductivity (σ_b) value has been calculated (using the formula Jonscher, and al, 1983), $\sigma_b = \frac{L}{S.R_b} (S.m^{-1})$

Where, R_b is bulk resistance of the sample, L is the thickness of the pellet, S is the area.

Table.3. Results obtained by the double law non-linear curve fitting by using origin Lab

Sample (LDH)	σ_{dc} (S/m)	A_1	n_1	A_2	n_2
Zn ₂ FeNO ₃	1.58E-06	1.69E-07	0.57	7.66E-11	0.91
Zn ₂ AlNO ₃	1.59E-07	1.02E-07	0.78	1.397E-10	0.86
Zn ₂ Fe _{0.5} Al _{0.5} NO ₃	5.06E-06	2.56E-06	0.52	1.724E-09	0.74

I.6.3. Electric Modulus

An alternate approach to analyze electrical relaxation is electric modulus. The electric modulus M^* can be defined in terms of the reciprocal of the complex dielectric constant $\epsilon^*(\omega)$ (Chandra babu and al 2011). In addition, the electrical modulus (M) is used to interpret the electrical properties minimizing large values of the permittivity and the conductivity at low frequency which can sometimes hide relaxations process (Louati.B and al 2014). Due to the foregoing, the formalism Modulus was chosen, and the complex modulus (M) was calculated from the complex impedance using the equation:

$$M^*(\omega) = Z_{i\omega C_0}^*(\omega).$$

The imaginary part of the dielectric modulus M'' as a function of frequency has been plotted in Fig. 11. The maximum in the $M''(\omega)$ at higher frequency region (Chandra babu and al 2011). At frequency above peak maximum $M''(\omega)$ determines the range in which charge carriers are spatially confined to potential wells, being mobile on short distances making only localized motion within the wells.

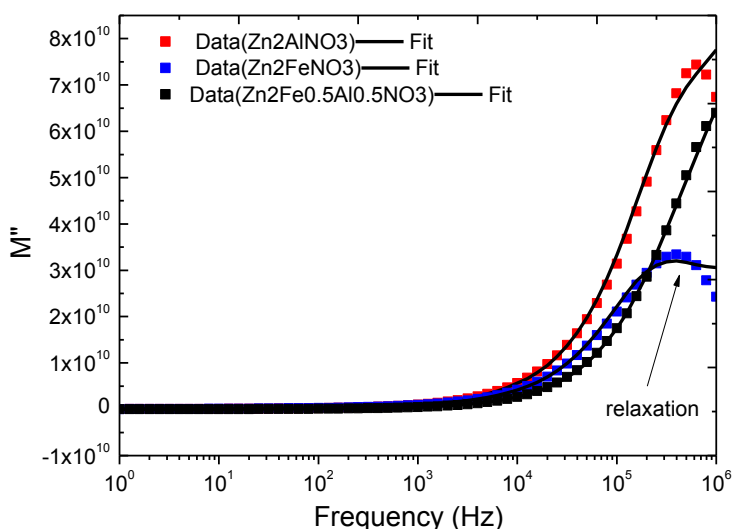


Figure 11: Variations of the imaginary part (M'') as a function of the frequency at ambient temperatures for Zn_2FeNO_3 , Zn_2AlNO_3 and $Zn_2Fe_{0.5}Al_{0.5}NO_3$

Conclusion:

In this work we presented impedance measurements on matrices of clays based on iron and aluminum. We show that the experimental and theoretical results are in good agreement.

These compounds have a very significant difference in point of view ac conductivity, particularly the dc conductivity of these compounds is compared it is estimated, using the values found by equivalent circuit at room temperature and low frequency are:

$$\sigma_{dc}(Zn_2Al_{0.5}Fe_{0.5}NO_3) > \sigma_{dc}(Zn_2FeNO_3) > \sigma_{dc}(Zn_2AlNO_3)$$

We see from this classification dc conductivity of the compound that has the best conductivity at low frequency direct current is that of the compound that contains iron and aluminum. For those of trivalent metal substitutions games in LDH we can increase the conductivity of the value $0.15\mu S/m$ as to the value $1.5\mu S/m$ that is to say a 10 times greater factor when clay contains only Al. The variation of M'' as a function of frequency shows the shifting of the peaks towards the high frequency as temperature increases which implies that there is a distribution of ionic relaxation time.

References

- A. Mantilla, F. Tzompantzi, J.L. Fernandez, J.A.I. Diaz G3ngora, G. Mendoza, R. Gomez,** Photo degradation of 2, 4-dichlorophenoxyacetic acid using Zn-Al-Fe layered double hydroxides as photo catalysts, *Catalysis Today* 148 (2009) 119–123
- A.S.Dzunuzvie, N.I.Ile, M.M Vijatovie Petrovie, J.D.Bodic, Z.Dohevie –Mitrove, B.D.Stojanovie.** Structure and properties of Ni–Zn ferrite obtained by auto-combustion method. *J. Magnetic Materials* 374(2015)245-251
- A. Ali Ahmed, Z.Talib, M. Ben Hussein.** Thermal, optical and dielectric properties of Zn–Al layered double hydroxide *Solid State Sciences* 14 (2012) 1196-1202.
- A. Langar , N. Sdiri , H. Elhouichet ,M. Ferid,** Conductivity and dielectric behavior of $NaPO_3-ZnO-V_2O_5$ glasses, *J. Alloys, Compounds* (2014)

- A. Elmelouky, R.Elmoznine, R.Lahkale, R.Sadik, E.SABBAR, E.Chahid, E.Choukri, D. Mezzane.** Analysis of conduction mechanism in lamellar double hydroxide by impedance spectroscopy. *J.Opt. Elect. Adv. Mater.* (2013), p. 1209-1216.
- A. Elmelouky, A.Mortadi, R. El Moznine, El. Chahid, R. Lahkale, El. Sabbar.** Analysis of Conduction Mechanism in Zn₂FeNO₃ using Impedance Spectroscopy. *International Journal of Advanced Research in Physical Science (IJARPS)*.2015, 2, 11: 1-10.
- Ajay Kumar Behera, Nilaya K. Mohanty, Banarji Behera, Pratibindhya Nayak,** Impedance properties of 0.7(BiFeO₃)-0.3 (PbTiO₃) composite, *Adv. Mat. Lett.* 2013, 4(2), 141-145
- EL. Chahid, R. EL Moznine, A. Zradba, A. Dani, A. Elmelouky, L. Idrissi; O. Cherkaoui, EL. Choukri, D.Mezzane, A. Belboukhari. J.** Optoelectronics. *Adv. Mater*, Vol. 15, No. 11 - 12, November – December 2013, p. 1209 – 1216.
- Chandra babu, B.; Naresh, V.; Jaya Prakash, B.; Buddhudu, S.** *Ferroelectrics Lett.* 2011, 38, 124.
- Louati, B.; Guindara, K.** Thermal and frequency dependance dielectric properties of conducting polymer / fly ash composites , *Adv. Mat. Lett.* 2014
- R. Allmann,** Doppelschicht strukturen mit brucit~ihnlichen Schichtionen $[M^{(II)}_{1-x}M^{(III)}_x(OH)_2]^{x+}$. *Chimia* 24 (1970) 99.
- H.Kavas, N.Kasapoglu, A.Baykal, Y.Koseoglu,** Characterisation of NiFe₂O₄nanoparticules synthetised by various methods. *Chimia, Pap.*63 (4) (2009) 450-455.
- Huebner, J.S., Dillenburg, R.G.** Impedance spectra of hot, dry silicate minerals and rock: qualitative interpretation of spectra. *American Mineralogist*, 46–64 (1995) 80.
- J. Yao, F. Wu, X. Qiu, N. Li, Y. Su.**Synthesis, electrical and dielectrical properties of lithium iron oxide, *Adv. Mater. Lett.* 2013, 4(4), 288-295
- Jonscher, A.K.** Dielectric relaxation in solids (Chelsea Press, London, 1983).
- M. Lakraimi, A. Legrouri, A. Barroug, A. De Roy, J. Besse.** Synthesis and characterisation of a new stable organo-mineral hybrid nonmaterial: 4-Chlorobenzenesulfonate in the Zinc–aluminum layered double hydroxide. (2006) 1763–1774
- P. Rosaiah, O. M. Hussain.** Synthesis, electrical and dielectrical properties of lithium iron oxide, *Adv. Mat. Lett.* 2013, 4(4), 288-295
- R.N. Singh, B.Lal, M.Malviya.** Electro-catalytic activity of electrode posited composite films of polypyrrole and CoFe₂O₄ nanoparticles towards oxygen reduction reaction. *Electrochimica Acta* 49(2004)4605-4612
- H. Roussel ,V. Briois ,E. Elkaim ,A. de Roy , and J. P. Besse.** Cationic Order and Structure of [Zn-Cr-Cl] and [Cu-Cr-Cl] Layered Double Hydroxides: A XRD and EXAFS Study. *J. Physical Chemistry B*, 2000.104(25) p. 5915 -5923.
- I Rousselot, C Taviot-Guého, F Leroux, P Léone, P Palvadeau, J Besse.** Insights on the Structural Chemistry of Hydrocalumite and Hydrotalcite-like Materials: Investigation of the Series Ca₂M³⁺(OH)₆Cl·2H₂O (M³⁺: Al³⁺, Ga³⁺, Fe³⁺, and Sc³⁺) by X-Ray Powder Diffraction. *J. Solid State Chemistry*, 2002.167(1) p. 137-144.
- V. Rives,** Layered Double Hydroxides: Present and Future, Nova Science, New-York, 2001;